



1 **BrGDGTs-based seasonal paleotemperature reconstruction for the last 15,000 years**
2 **from a shallow lake on the eastern Tibetan Plateau**

3 Xiaohuan Hou ^a, Nannan Wang ^a, Zhe Sun ^b, Kan Yuan ^{a,c}, Xianyong Cao ^a, Juzhi Hou ^{a*}

4 ^a *Group of Alpine Paleoecology and Human Adaptation (ALPHA), State Key Laboratory of Tibetan*
5 *Plateau Earth System, Resources and Environment (TPESRE), Institute of Tibetan Plateau Research,*
6 *Chinese Academy of Sciences, Beijing 100101, China*

7 ^b *Institute of Geography and Resources Science, Sichuan Normal University, Chengdu, 610066, China*

8 ^c *University of Chinese Academy of Sciences, Beijing 100049, China*

9

10 * Corresponding author

11 E-mail address: houjz@itpcas.ac.cn

12



13 **ABSTRACT**

14 Knowledge of Holocene temperature changes is crucial for addressing the problem of the
15 discrepancy between Holocene proxy temperature reconstructions and climate model
16 simulations. The complex spatiotemporal pattern of temperature variations on the Tibetan
17 Plateau (TP) further complicates the study of Holocene continental climate change. The
18 discrepancy between model-based and proxy-based Holocene temperature reconstructions
19 possibly results from the seasonal biases and environmental ambiguities of the proxies.
20 Quantitative temperature reconstructions using different proxies from the same sediment core
21 can provide an effective means of evaluating different proxies; however, this approach is
22 unusual in terrestrial environments. Here, we present an ice-free-season temperature record
23 for the past 15 ka from a shallow, freshwater lake on the eastern TP, based on brGDGTs
24 (branched glycerol dialkyl glycerol tetraethers). This record shows that the Holocene Thermal
25 Maximum lags the pollen-based July temperature recorded in the same sediment core. We
26 conclude that the mismatch between the brGDGTs-based and pollen-based temperatures is
27 primarily the result of seasonal variations in solar irradiance. The overall pattern of
28 temperature changes is supported by other summer temperature records, and the Younger
29 Dryas cold event and the Bølling–Allerød warm period are also detected. A generally warm
30 period occurred during 8–3.5 ka, followed cooling in the late Holocene. Our findings have
31 implications for understanding the seasonal signal of brGDGTs in shallow lakes, and provide
32 critical data for confirming the occurrence of seasonal biases in different proxies from high-
33 elevation lakes. To further investigate the significance of the brGDGTs and temperature
34 patterns on the TP, we reviewed previously published brGDGTs-based Holocene temperature



35 records across the TP. The results demonstrate that brGDGTs can record both annual mean
36 temperature and a warm-biased temperature, and that both show a gradual warming trend
37 during the Holocene with relatively cooler conditions during the middle Holocene, and a
38 cooling trend during the middle to late Holocene. We analyzed the possible reasons for the
39 diverse brGDGTs records on TP and emphasize the importance of considering lake
40 conditions and modern investigations of brGDGTs in lacustrine systems when using
41 brGDGTs to reconstruct paleoenvironmental conditions.

42 **Keywords:** Tibetan Plateau, brGDGTs, warm-biased temperature, shallow lake, Holocene

43 **1 Introduction**

44 Global climate change has had a profound impact on both the natural ecological and socio-
45 economic systems that are vital for human survival and development, making climate change
46 a critical limiting factor for the sustainable development of human society. The Tibetan
47 Plateau (TP), also called the “Third Pole” (Qiu, 2008), has undergone rapid warming over the
48 last five decades, with a rate twice that of the global average (0.3 – 0.4°C/decade) (Chen et al.,
49 2015; Kuang and Jiao, 2016), making it one of the world's most temperature-sensitive regions
50 (Chen et al., 2015; Yao et al., 2022). Consequently, assessing the impact of future climate
51 change on the TP is becoming increasingly important. To enhance the precision and accuracy
52 of future climate change estimates for the TP under ongoing global climate change and to
53 minimize the uncertainty in climate simulations, it is essential to investigate the processes and
54 mechanisms of regional climate and environmental changes, with particular emphasis on
55 temperature, on a relatively long timescale, such as that of the Holocene.
56



57 The Holocene, the most recent geological epoch, is closely linked with the development of
58 human civilization. Quantitative reconstructions of Holocene temperature trends can be used
59 to explore their impacts on civilization and to establish a geological and historical context for
60 predicting future climate changes. In recent decades, several Holocene quantitative
61 reconstructions of seasonal and annual temperatures for the TP have been produced using
62 various proxies, like pollen (Lu et al., 2011; Herzschuh et al., 2014), chironomids (Zhang et
63 al., 2017; Zhang et al., 2019a), $\delta^{18}\text{O}$ in ice deposits (Thompson et al., 1997; Pang et al., 2020),
64 and biomarkers (Zhao et al., 2013; Hou et al., 2016; Cheung et al., 2017). These
65 reconstructions have provided crucial data for the elucidation of Holocene temperature
66 changes. However, the available Holocene temperature records from the TP show divergent
67 trends. Multiple proxy indicators indicate three different Holocene temperature patterns on
68 the TP. First, a consistent Holocene warming trend (Opitz et al., 2015; Feng et al., 2022; Sun
69 et al., 2022). For example, brGDGTs based annual temperatures (Feng et al., 2022; Sun et al.,
70 2022) indicate a gradual warming trend which resembles the $\delta^{18}\text{O}$ temperature record from
71 the Chongce ice core on the western TP, except for the last 2 ka (Pang et al., 2020). Second,
72 an early to middle Holocene summer temperature maximum and a gradual cooling trend
73 during the late Holocene are observed in pollen-, alkenone- and chironomid-based
74 temperature records (Herzschuh et al., 2014; Zheng et al., 2015; Hou et al., 2016; Zhang et al.,
75 2017; Wang et al., 2021a). Third, a prominent relatively cool middle Holocene (Li et al., 2017;
76 Wang et al., 2021c); for example, a composite temperature record suggests that temperatures
77 were $\sim 2^\circ\text{C}$ cooler during the middle Holocene than during the early and late Holocene (Wang
78 et al., 2021c). Several records also show a steady long-term trend without distinct cooling or



79 warming (Sun et al., 2021). Moreover, the cooling trends in proxy-based Holocene
80 temperature records are inconsistent with those of climate models, which indicate a warming
81 trend, and this inconsistency is widely known as the “Holocene temperature conundrum” (Liu
82 et al., 2014). There are several potential factors that may contribute to the disparity in
83 Holocene temperature trends, including seasonal biases and uncertainties in temperature
84 proxies and reconstructions, independent of climate models (Liu et al., 2014; Marsicek et al.,
85 2018; Hou et al., 2019; Bova et al., 2021; Cartapanis et al., 2022). While several recent
86 studies have suggested that seasonality in proxies is not the major cause of the Holocene
87 temperature conundrum (Dong et al., 2022; Zhang et al., 2022b), it is significant that the TP
88 is an alpine and high-altitude region with significant seasonal temperature variations.
89 Moreover, most organisms tend to grow during the warmer seasons at high latitudes and high
90 altitudes (Zhao et al., 2021a). Currently, however, we lack unambiguous and reliable seasonal
91 temperature records to support a seasonality-bias hypothesis. Most previous studies have
92 relied on a single temperature proxy, and the few studies that have used multiple proxies from
93 the same sediment core have tended to focus on annual average temperature and summer
94 temperature. For example, a chironomid-based July temperature reconstruction for Tiancai
95 lake on the southeastern TP shows higher temperatures during the early to middle Holocene
96 (Zhang et al., 2017), while the brGDGTs-based annual average temperature shows a warming
97 trend (Feng et al., 2022). Different proxies may reflect the seasonal temperatures in different
98 months, and thus producing temperature reconstructions for different months for the same
99 sediment core may help better understand the seasonal bias of terrestrial temperature records.
100 Furthermore, the reconciliation of the divergent trends of Holocene temperature on the TP



101 and its surroundings requires additional high-altitude temperature records from these regions,
102 with reliable chronologies and proxy records with an unambiguous climatological
103 significance.

104

105 Branched glycerol dialkyl glycerol tetraethers (brGDGTs) are a group of membrane-spanning
106 lipids found in bacteria (Fig. S1) (Damsté et al., 2000; Chen et al., 2022; Halamka et al.,
107 2022), and they have become a powerful tool for quantifying past terrestrial temperature
108 variations. Through investigations of brGDGTs in globally-distributed soils, it was found that
109 the distribution of brGDGTs is primarily related to temperature and pH (Weijers et al., 2007).
110 Subsequently, brGDGTs–temperature calibrations from soil, peat and lake sediments were
111 established on scales from global (Weijers et al., 2007; De Jonge et al., 2014; Crampton-
112 Flood et al., 2020; Martínez-Sosa et al., 2021) to regional (e.g., East Asia) (Sun et al., 2011;
113 Ding et al., 2015; Wang et al., 2016; Dang et al., 2018), leading to significant progress in
114 reconstructing terrestrial temperatures, particularly on the TP (Zhao et al., 2013; Cheung et
115 al., 2017; Li et al., 2017; Zhang et al., 2022a).

116

117 Natural lakes are widely distributed across the TP (Zhang et al., 2019b). Lake sediments are
118 often organic matter-rich and they accumulate continuously and rapidly, providing high
119 resolution records of environmental change, and they are thus regarded as the most important
120 terrestrial climate archive (Moser et al., 2019). BrGDGTs in lacustrine systems are often
121 more strongly correlated with temperature, with higher coefficient of determination (r^2) and
122 lower root mean square error (RMSE) values (Martínez-Sosa et al., 2021), than in soils and



123 peats. However, the factors influencing the distribution of brGDGTs in lakes are complex and
124 multidimensional; moreover, as well as temperature and pH, other factors like salinity (Wang
125 et al., 2021b), oxygen content (Buckles et al., 2014a), and water depth (Woltering et al., 2012)
126 can significantly impact the distribution of brGDGTs in lakes.

127

128 In this study, we obtained a quantitative temperature reconstruction for the past 15 ka from
129 Gahai, a shallow (average depth of ~2 m) freshwater lake located in the source area of the
130 Yellow River. This region is an important ecological protection area on the eastern edge of
131 the TP. Freshwater environments avoid the confounding effects of salinity on brGDGTs-
132 based temperature reconstructions, and shallow lakes also minimize the impact of the uneven
133 distribution of light and nutrients on brGDGTs. Our specific aims were: (1) to determine the
134 long-term trend of Holocene warm-biased terrestrial temperatures at a high elevation; (2) to
135 compare records of ice-free season temperatures with July temperatures from the same
136 sediment core; and (3) to gain a better understanding of the possible mechanisms responsible
137 for Holocene temperature variations, especially on the TP.

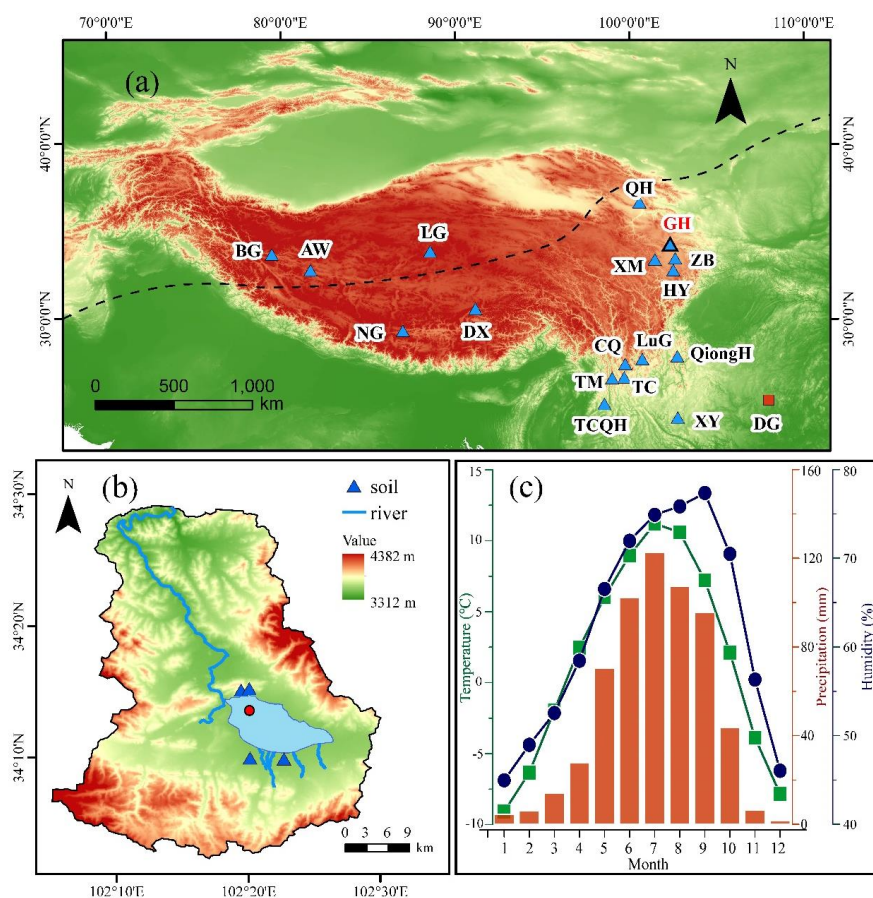
138 **2 Materials and methods**

139 *2.1 Study site*

140 Gahai (102°11'–102°28' E, 34°04'–34°4' N, 3444 m a.s.l.) is a freshwater lake and part of the
141 Gahai meadow wetland, which is a national nature reserve with restricted human access, on
142 the eastern edge of the Tibetan Plateau (Fig. 1). The lake is fed by runoff from the
143 surrounding hills, and it drains into the Tao river, which ultimately enters the Yellow river.
144 Thus, Gahai lake is a critical water conservation area in the upper reaches of the Yellow River.



145 The average water depth of Gahai is ~1–2 m, and the maximum depth is ~5 m. The
146 vegetation in the catchment consists mainly of *Kobresia tibetica*, *Equisetum arvense*,
147 *Potentilla anserina*, *Artemisia subulate*, and *Oxytropis falcata* (Ma et al., 2019).
148 Meteorological data for the area are available from Langmu Temple station (Fig. 1) (102°38'
149 E, 34°5' N, 3412 m a.s.l.), ~32 km northwest of Gahai lake. They indicate an annual average
150 (mean) precipitation of 781 mm, with > 67% occurring between June and September, and
151 mean annual temperature of 1.2 °C with a relative humidity of ~65%. The summers are mild
152 and humid and the winters are cold and dry. From May to September, the mean average
153 temperature is above freezing (0°C), but the temperature in May is very low, close to 0°C.



154

155 **Fig. 1** (a) Locations of the sites on the Tibetan Plateau referenced in the text. Triangle with
156 bold line indicates the location of Gahai lake (this study). Other triangles indicate the
157 locations of cited studies on the Tibetan Plateau and the surrounding area: Bangong Co
158 (BG), Aweng Co (AW), Ngamring Co (NG), Linggo Co (LG), Dangxiong wetland (DX),
159 Qinghai lake (QH), Ximen Co (XM), Zoige Basin (ZB), Hongyuan peatland (HY), Lugu
160 lake (LuG), Cuoqia lake (CQ), Tingming lake (TM), Tengchongqinghai lake (TCQH),
161 Tiancai lake (TC), Qionghai lake (QH), Xingyun lake (XY). Red square indicates
162 Dongge Cave (DG). Black dotted line represents the northern boundary of the modern
163 Asian summer Monsoon (Chen et al., 2008). (b) Drainage basin of Gahai lake and the
164 core site. (c) Climate data from Langmu Temple meteorological station: monthly
165 temperature (green line), precipitation (red bars), and humidity (blue line).



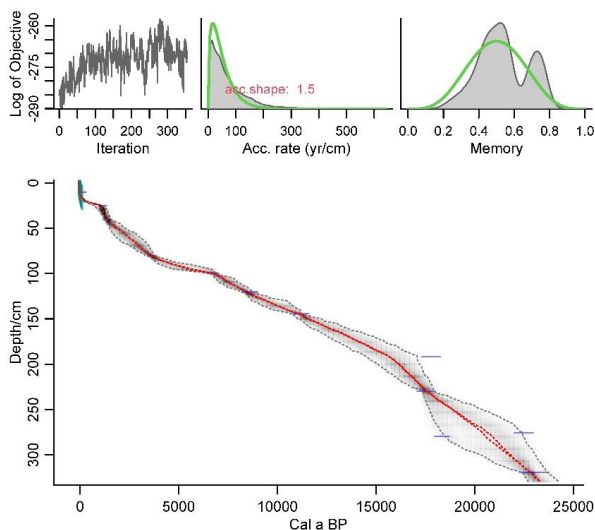
166 2.2 Sampling

167 A sediment core with the length of 329 cm was obtained from Gahai Lake in January 2019, at
168 a water depth of 1.95 m, using a UWITEC platform operated from the frozen lake surface. In
169 addition, several catchment soil samples were collected from around the lake (Fig. 1). All
170 samples were transported to the Institute of Tibetan Plateau Research, Chinese Academy of
171 Sciences (ITPCAS). The sediment core was split lengthwise, and one half was subsampled
172 and freeze-dried for subsequent analysis.

173

174 2.3 Chronology

175 The chronology of the upper 20 cm of the sediment core is based on measurements of ^{210}Pb
176 and ^{137}Cs , at a 1-cm interval. The chronology for the deeper part of the core is provided by
177 accelerator mass spectrometry (AMS) ^{14}C measurements of 13 bulk sediment samples, which
178 were conducted by Beta Analytic Inc. (Miami, USA) (Fig. 2) (Wang et al., 2022).



179

180 **Fig. 2** Age-depth model for Gahai, based on AMS ^{14}C , ^{210}Pb and ^{137}Cs ages (Wang et al.,

181 2022). The ages of the upper 20 cm are based on ^{210}Pb and ^{137}Cs dating (green symbols)



182 and those of the lower part on AMS ^{14}C dates (blue symbols).

183

184 *2.4 Lipids extraction and brGDGTs analysis*

185 For lipids extraction, ~5 g samples were ground to a powder and extracted ultrasonically with
186 dichloromethane (DCM): methanol (MeOH) (9: 1, v: v) three times. The supernatants were
187 combined and dried under a stream of nitrogen gas. Subsequently, the total lipid extracts were
188 separated into neutral and acid fractions through a LC-NH₂ silica gel column using DCM:
189 isopropyl alcohol (2: 1, v: v) and ether with 4% acetic acid (v: v), respectively. The neutral
190 fraction was then eluted through a silica gel column using n-Hexane, DCM and MeOH, and
191 the GDGTs were dissolved in the MeOH. The GDGTs fraction was passed through a 0.45 μm
192 polytetrafluoroethylene (PTFE) filter before analysis. C₄₆-GDGT (a standard compound)
193 ([Huguet et al., 2006](#)) was added to the samples before analysis.

194

195 BrGDGTs were detected using an HPLC-APCI-MS (Waters ACQUITY UPLC I-Class/Xevo
196 TQD) with auto-injection at the ITPCAS. The compounds were separated by three Hypersil
197 Gold Silica LC columns in sequence (each 100 mm \times 2.1 mm, 1.9 μm , Thermo Fisher
198 Scientific; USA), maintained at a temperature of 40°C. GDGTs were eluted isocratically
199 using 84% hexane and 16% ethyl acetate (EtOA) for the first 5 min, followed by a linear
200 gradient change to 82% hexane and 18% EtOA from 5 to 65 min. The columns were cleaned
201 using 100% EtOA for 10 min, and then back to 84% hexane and 16% EtOA to equilibrate the
202 column, with a flow rate of 0.2 ml min⁻¹.

203



204 The APCI-MS conditions were as follows: nebulizer pressure at 60 psi, APCI probe
205 temperature at 400°C, drying gas flow rate of 6 L/min and temperature of 200°C, capillary
206 voltage of 3600 V, source corona of 5.5 μ A. Detection was performed in selected ion
207 monitoring (SIM) mode, targeting the protonated molecules at m/z 1050, 1048, 1046, 1036,
208 1034, 1032, 1022, 1020, 1018 and 744. The results were analyzed using MassLynx V4.1
209 software, and quantification was achieved by comparing the peak areas of targeted ions and
210 the internal standard, assuming an identical response factor for GDGTs.

211

212 **3 Results and Discussion**

213 *3.1. Concentration and distribution of brGDGTs in the sediment core and catchment soils*

214 BrGDGTs were detected in both the catchment soils and the downcore sediments. The
215 average concentration of brGDGTs in the catchment soils (0.07 ng g⁻¹dw) was significantly
216 higher than in the surficial core sediments (0.70 ng g⁻¹dw). In the soil samples,
217 pentamethylated brGDGTs were generally the most abundant (55.33%), followed by
218 tetramethylated brGDGTs (23.60%) and hexamethylated brGDGTs (21.07%) (Fig. S2). The
219 relative amount of cyclopentane ring-containing brGDGTs in the soil samples was generally
220 low (24.34%) and it was sometimes too low to be detected, especially the fractions of IIIb,
221 IIIb', IIIc, IIIc', IIc and IIc'. In the downcore sediments, the relative abundance of
222 tetramethylated brGDGTs (43.84%) was like that of pentamethylated brGDGTs (41.93%),
223 and hexamethylated brGDGTs were the least abundant (14.22%) (Fig. S2). The relative
224 abundant of cyclopentane ring-containing brGDGTs in the downcore sediments (67.82%)
225 was lower than that in the catchment soils.

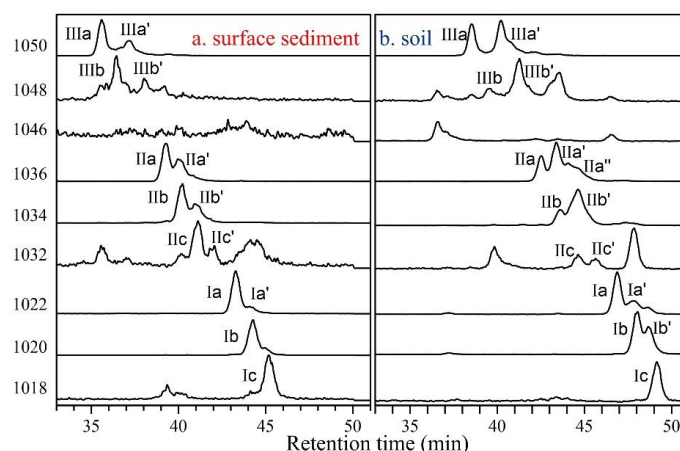


226 *3.2 In situ production of brGDGTs in Gahai lake*

227 Although lacustrine brGDGTs have great potential for quantitatively reconstructing terrestrial
228 paleotemperatures, uncertainties about their sources in lacustrine environments are a major
229 factor limiting their application (Damsté et al., 2009; Tierney and Russell, 2009; Sun et al.,
230 2011; Buckles et al., 2014b; Cao et al., 2020). To investigate the origin and characteristics of
231 brGDGTs in the Gahai lake sediments, we examined the distributions and concentrations of
232 brGDGTs in the sediments and catchment soils and found significant differences between
233 them. First, as described in the previous section, the average content of brGDGTs in the
234 catchment soils was ~10% that of the surficial lake sediments, suggesting the absence of
235 large-scale allochthonous inputs from the catchment soils. Second, the brGDGTs distributions
236 in the downcore sediments were quite different from those in the catchment soils, which
237 suggests a significant autochthonous brGDGTs contribution to the lake sediments (Fig. 3 and
238 Fig. S2). Moreover, the ratios of 6-methyl brGDGTs to 5-methyl GDGTs (IR_{6ME}) in the soils
239 and sediments, calculated according to the formula proposed by De Jonge et al. (2014), were
240 significantly different. In the soil samples, IR_{6ME} varied between 0.54 and 0.57 and the
241 average ratio in the downcore samples was 0.26, varying between 0.18 and 0.47. Third, the
242 in-situ production of brGDGTs in Gahai lake is suggested by the discrepancies in the degree
243 of methylation (MBT'_{5ME}) between the soils and surface sediments. The average value of
244 MBT'_{5ME} in the Gahai lake surface sediments was 0.48, which is clearly higher than in the
245 catchment soils, with the range of 0.32–0.35. Fourth, and potentially the most significant, the
246 IIIb' and Ib' compounds are present in the catchments soil but not in the Gahai lake surficial
247 sediments, which may be direct evidence of an autochthonous brGDGTs contribution in the



248 lacustrine environment (Fig. 3), and a lower proportion of soil-derived brGDGTs input.
249 Therefore, we conclude that the brGDGTs in the Gahai lake sediments are mainly of in-situ
250 origin.



251

252 **Fig. 3** Representative high-performance liquid chromatography/atmospheric pressure
253 chemical ionization-mass spectrometry (HPLC/APCIMS) chromatograms of brGDGTs
254 from (a) surface sediments from Gahai lake, and (b) soils in the catchment of Gahai lake.

255

256 3.3 brGDGTs-temperature calibration and Holocene temperature reconstruction

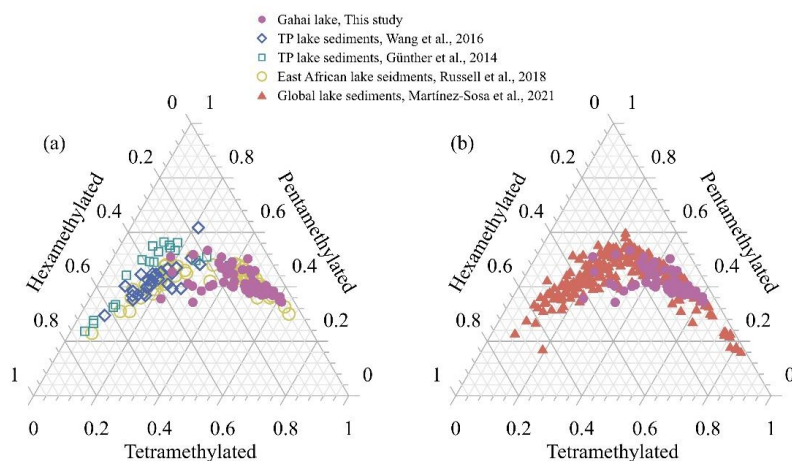
257 Given the substantial contribution of authigenic brGDGTs in the Gahai lake sediments, we
258 reconstructed the Holocene paleotemperature record using previously published lake-specific
259 brGDGTs-temperature calibrations (e.g., Sun et al., 2011; Günther et al., 2014; Wang et al.,
260 2016; Dang et al., 2018; Russell et al., 2018; Martínez-Sosa et al., 2021). As shown in Fig. S3,
261 most calibrations produced qualitatively similar patterns of temperature change when applied
262 to the sediment core from Gahai lake, but the amplitudes vary considerably. Among these
263 calibrations, the reconstruction based on Martínez-Sosa et al. (2021) was chosen to produce



264 the final result, for several reasons. We compared the fractional abundances of summed tetra-,
265 penta- and hexamethylated brGDGTs of Gahai lake with other datasets (Fig. 4), including
266 lake sediments from the Tibetan Plateau (Günther et al., 2014; Wang et al., 2016), East Africa
267 (Russell et al., 2018), and global lakes (Martínez-Sosa et al., 2021). The fraction plot of the
268 Gahai core sediments is clearly distinct from the other Tibetan Plateau lake-sediments, even
269 though they are all from the same region (Fig. 4), likely because the brGDGTs in Tibetan
270 lakes are mainly soil-derived (Wang et al. (2016). Moreover, the novel analytical technique
271 for separating 5- and 6-methyl isomers was not used in the studies of Wang et al. (2016) and
272 Günther et al. (2014), and thus these two calibrations were excluded. The fractional
273 distribution of brGDGTs in Gahai lake is spanned by that of global lakes, and based on
274 multiyear observed temperature records from the nearest meteorological station, the modern
275 mean temperature of the months with temperatures above freezing in Gahai lake (May to
276 September) was 8.8°C, which is like the brGDGT-inferred temperature for the surficial
277 sediments (9.4°C), obtained using the calibration of Martínez-Sosa et al. (2021). However,
278 the annual mean temperature reconstructed according to Russell et al. (2018) differs
279 significantly from that from Langmu Temple station, although the characteristics of the Gahai
280 brGDGTs fractions resemble those of East African lakes. The paleotemperature
281 reconstruction for Gahai lake based on the warm season-temperature calibration proposed by
282 Dang et al. (2018) is similar to that of Martínez-Sosa et al. (2021); however, this calibration
283 was established based on an investigation of 35 Chinese alkaline lakes, in contrast to
284 freshwater Gahai lake. Similarly, although the salinity effect was corrected, the calibration
285 reported by Wang et al. (2021b) is not considered here. Therefore, we used a new Bayesian



286 calibration for the mean temperature of the Months Above Freezing (Martínez-Sosa et al.,
287 2021) to reconstruct a warm-biased temperature for Gahai lake.



288

289 **Fig. 4** Comparison of the fractional abundances of tetramethylated, pentamethylated, and
290 hexamethylated bGDGTs in sediment core samples from Gahai with lake surface
291 sediments from the Tibetan Plateau (Günther et al., 2014; Wang et al., 2016), East Africa
292 (Russell et al., 2018), and worldwide (Martínez-Sosa et al., 2021).

293

294 Many studies have suggested that lacustrine brGDGTs-derived temperatures are likely to
295 have a warm season bias, especially in cold regions at middle to high latitudes (Shanahan et
296 al., 2013; Peterse et al., 2014; Dang et al., 2018; Cao et al., 2020). However, for lakes in
297 warmer regions, the reconstructed temperatures are much closer to the annual average
298 temperature (Tierney et al., 2010; Loomis et al., 2012). Gahai is a shallow lake that is usually
299 completely frozen during winter and spring, and the local meteorological data show that the
300 average snowfall period is 269 days, and that the snowfall period lasts for ~50 days. Thus, the



301 light transmittance and oxygen content during the lake water freezing season at Gahai are
302 reduced, as well as the lake water nutrient contents, which seriously inhibit the growth of
303 autotrophic microorganisms. Although the bacteria that produce brGDGTs are not well
304 characterized, heterotrophic bacteria will be reduced by the decreased autotrophic biomass.
305 Therefore, we suggest that the brGDGTs-based temperatures from Gahai are biased towards
306 the growing season (summer and autumn).

307

308 The depth interval of 191–279 cm in the Gahai sediment core represents an interval of rapid
309 allocthonous sedimentation, or alternatively a slump, and therefore the results for the
310 corresponding time interval of 20–15 ka may be unreliable. Thus, our warm-biased
311 temperature record from the eastern TP spans the past 15 ka, with the average temperature of
312 4°C, as shown in Fig. 5a. Weak warming occurred during 14.8–11.8 ka which coincides with
313 the Bølling–Allerød (B/A) interstadial, and a minor cold reversal occurred during 11.8–10.5
314 ka, which approximates the Younger Dryas (YD). The temperature record indicates a colder
315 period during 11.5–8.0 ka. During 8.0–3.5 ka, Gahai experienced a stable warm period with
316 the average temperature of ~16.5°C, after which the temperature decreased gradually. Overall,
317 the maximum temperature difference since 15 ka was ~10°C. The interval of 11.5–10.5 ka is
318 represented by a relatively low number of samples because the concentration of brGDGTs
319 was below the detection limit.

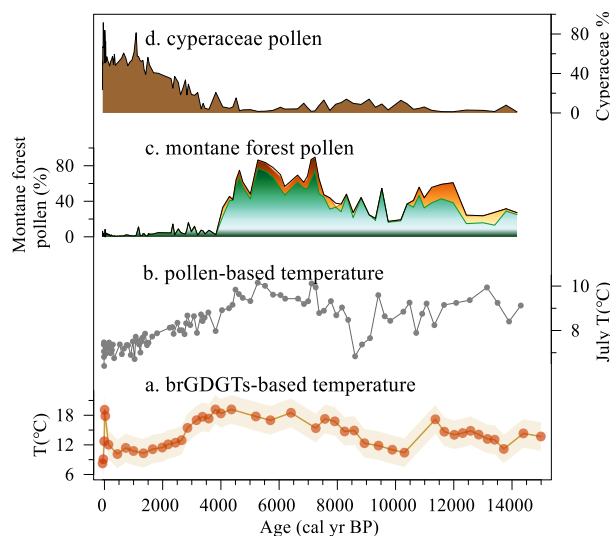
320

321 *3.4 Holocene temperature changes on the eastern edge of TP and their origin*

322 Despite the difference in amplitude, the warm-biased temperature record from Gahai



323 resembles the pollen record and the pollen-based temperature reconstruction from the same
324 site (Fig. 5) (Wang et al., 2022). However, the brGDGTs-based Holocene Thermal Maximum
325 (HTM) lags the pollen-based reconstruction (Fig. 5a, b). Wang et al. (2022) used a weighted-
326 averaging partial least regression approach to produce a temperature record for Gahai, based
327 on a modern pollen dataset (n=731) from the eastern TP. Assessment of the statistical
328 significance of the pollen-based climate variables for Gahai suggests that the mean July
329 temperature is the most important environmental factor influencing the fossil pollen
330 assemblages. The brGDGTs in Gahai are indicative of summer and autumn temperatures, and
331 the mismatch between the temperature records inferred from brGDGTs and the pollen record
332 may be attributed to the difference between the solar irradiance during June–October and that
333 during July. Additionally, significant vegetation changes occurred in the Gahai area during
334 4.0–3.5 ka, when the dominant high-elevation montane forest was rapidly replaced by alpine
335 steppe. The poor vegetation coverage and lower soil moisture level during this period (Fig. 5c,
336 d) (Wang et al., 2022) would have resulted in more efficient heat absorption, causing surface
337 warming (Lu et al., 2019).



338

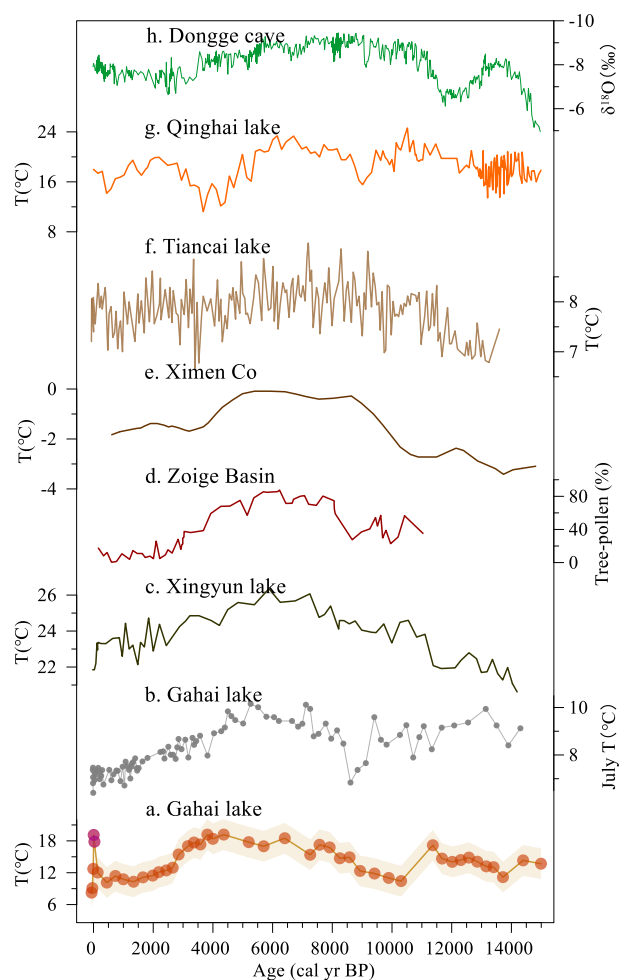
339 **Fig. 5** Comparison of multiproxy records from Gahai lake. (a) brGDGTs-based warm-bias
340 temperature (this study). (b) Temperature of the warmest month (July) based on pollen
341 assemblages (Wang et al., 2022). (c, d) Pollen-reconstructed montane forest (*Pinus*,
342 *Picea*, *Abies*) and Cyperaceae pollen record (Wang et al., 2022).

343

344 The brGDGTs-based temperature record from Gahai is also consistent with several other
345 pollen and pollen-reconstructed temperature records from the eastern TP (Fig. 6), suggesting
346 that it is a reliable representation of Holocene temperature changes in this region. For
347 example, pollen-based temperature reconstructions from Xingyun lake and Ximen Co on the
348 eastern TP show a early to middle HTM (9–4 ka) and a cooling trend thereafter (Fig. 6c, e)
349 (Herzschuh et al., 2014; Wu et al., 2018; Wang et al., 2021a). Additionally, lake water
350 temperature reconstructions based on subfossil chironomids from Tiancai lake (Fig. 6f)
351 (Zhang et al., 2017; Zhang et al., 2019a) and alkenones from Qinghai lake (Fig. 6g) (Hou et
352 al., 2016) show the same trends during the past 15 ka, as also shown by other pollen-based



353 temperature records from the TP (Chen et al., 2020). Pollen, chironomids and alkenones
354 mainly respond to the growing season temperatures in middle and high latitudes, and thus the
355 reconstructed temperature records are consistent with the variations in summer solar
356 irradiance. Similar variations were documented in temperature reconstructions at a global
357 scale (Marcott et al., 2013; Cartapanis et al., 2022).



358

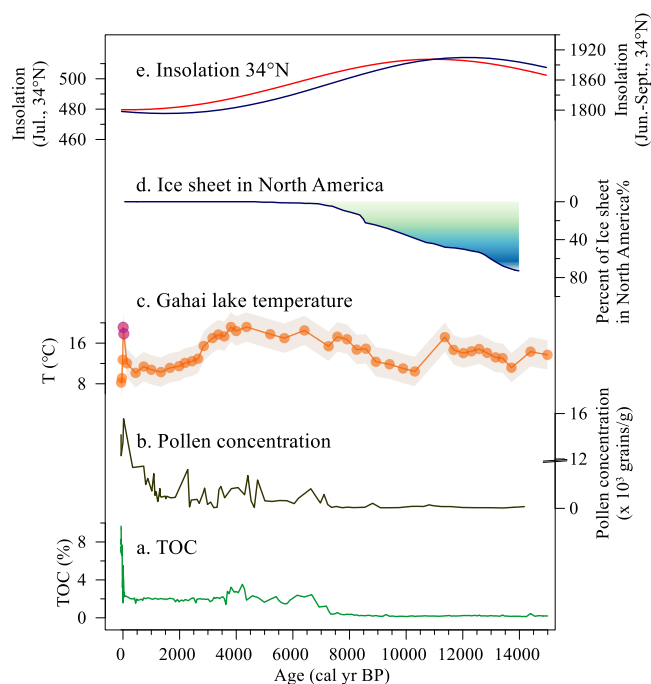
359 **Fig. 6** Comparison of temperature at Gahai and other records from the eastern edge of the
360 Tibetan Plateau. (a) brGDGTs-based warm-bias temperature at Gahai, the purple dots
361 may indicate unreliable temperature changes influenced by human activities (this study).



362 (b) Temperature of the warmest month (July) based on pollen data from Gahai (Wang et
363 al., 2022). (c) Pollen-based temperature at Xingyun lake (Wu et al., 2018). (d) Tree
364 pollen percentages from the Hongyuan peatland in the southern Zoige Basin (Zhou et al.,
365 2010). (e) Pollen-based temperature at Ximen Co (Herzschuh et al., 2014). (f)
366 Chironomid-based temperature at Tiancai lake (Zhang et al., 2017, 2019a). (g)
367 Alkenone-based temperature at Qinghai lake (Hou et al., 2016). (h) Stalagmite $\delta^{18}\text{O}$
368 record of Dongge cave (Dykoski et al., 2005).

369

370 Nevertheless, the timing and amplitude of the Gahai temperature fluctuations differ from
371 those of other temperature records from this region (Fig. 6). These discrepancies may be the
372 result of the chronological uncertainties of these records, and to differences in the seasonal
373 and spatial responses to climate forcing and feedbacks. The temperature records shown in Fig.
374 6 mostly refer to summer temperatures, which are primarily influenced by summer insolation.



375



376 **Fig. 7** Temperature fluctuations and forcing factors during the Holocene. (a, b) TOC content
377 and pollen concentrations from Gahai (Wang et al., 2022). (c) brGDGTs-based warm-
378 bias temperature from Gahai, the purple dots may indicate unreliable temperature
379 changes influenced by human activities (this study). (d) Percentage of the remnant
380 Laurentide ice sheet in North America relative to the Last Glacial Maximum (Dyke,
381 2004). (e) Local insolation at 34 °N during ice-free months (Laskar et al., 2004).

382

383 The warm-biased temperature record in Gahai during the early Holocene fails to closely track
384 the Northern Hemisphere insolation trend, and there is also a time lag. The pollen-based
385 temperature record for Xingyun Lake in southwestern China also shows lower temperatures
386 in the early Holocene (Fig. 6c). The albedo effect caused by the increased cloud cover may be
387 the reason for the early Holocene decrease in summer temperatures (Wu et al., 2018).
388 However, the pollen record from Gahai indicates dry conditions during the early Holocene
389 (Wang et al., 2022), and cloud cover may not be the primary factor responsible for the low
390 temperatures at this time. The melting of Northern Hemisphere ice sheets during the early
391 Holocene weakened the Atlantic Meridional Overturning Circulation (AMOC) and
392 potentially also the global thermohaline circulation. This led to a reduction in the amount of
393 heat transport by the North Atlantic warm current to high-latitude regions, which resulted in
394 the low temperatures in middle to high latitudes of the Northern Hemisphere. The persistence
395 of the Laurentide ice sheet into the early Holocene maintained the regional albedo, as well as
396 discharging meltwater into the North Atlantic (Fig. 7d) (Dyke, 2004). It is possible that these
397 factors impacted the summer temperatures in the Indian Summer Monsoon (ISM) domain via



398 ocean-atmosphere interactions. In addition, a Holocene temperature simulation showed that
399 global warming was more pronounced when dust factors were excluded from the simulation
400 (Liu et al. (2018)). The record of insoluble particles in the Greenland GISP2 ice core indicates
401 relatively high concentrations of atmospheric aerosols in the early Holocene (Zielinski and
402 Mershon, 1997), which would have weakened summer solar irradiation via radiative
403 feedback, leading to the cool temperatures during this period. These factors may together
404 have caused the early Holocene temperature decline at Gahai Lake, which slightly delayed
405 the onset of the Holocene Warm Period.

406

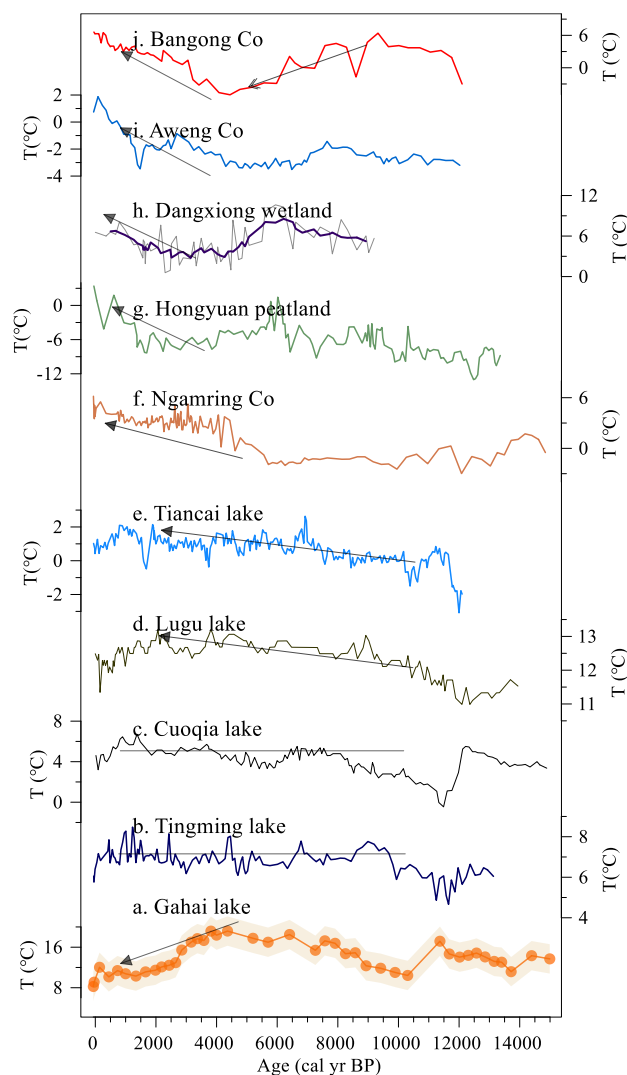
407 A significant and rapid temperature increase is evident at Gahai in recent decades, which
408 differs significantly from the other records (Fig. 7c). Moreover, there are notable increases in
409 pollen concentration, TOC, and TN (Fig. 7a, b) in the Gahai sediment core, indicating
410 intensive local human activities like grazing and tourism, which may be the primary cause of
411 the environmental changes in this region (Wang et al., 2022). This intensive human activity
412 may have reduced the ability of the brGDGTs to record the natural temperature background.
413 However, a series of environmental protection measures, including the government-enforced
414 exclusion of grazing, and a grassland restoration program, have been implemented to restore
415 the natural ecological environment of this area. Consequently, the brGDGTs-based
416 temperature record decreased rapidly within the modern era, returning to normal levels, and it
417 may provide a reliable regional record of the warm season temperature. These observations
418 emphasize the significant impact of human activities on climate proxies and the need to
419 carefully consider their effect on temperature reconstructions.



420

421 *3.5 Spatiotemporal pattern of brGDGTs-based TP temperatures*

422 In addition to comparing the Gahai temperature with the summer temperature records from
423 the eastern TP and its surrounding areas, we compiled and reviewed published Holocene
424 brGDGTs-based quantitative temperature records from across the TP. As shown in [Fig. 8](#),
425 with the increasing number of these records for the TP, the differences between the results
426 have become more pronounced. The brGDGTs records from lakes in the central and western
427 parts of the plateau show higher temperatures in the early and late Holocene, and lower
428 temperatures in the middle Holocene ([Li et al., 2017](#); [He et al., 2020](#); [Wang et al., 2021c](#)),
429 while the brGDGTs records from lakes in the southern and south-eastern parts of the TP show
430 a warming trend throughout the Holocene ([Feng et al., 2022](#); [Sun et al., 2022](#)). In addition,
431 brGDGTs in Cuoqia lake and Tingming lake, on the south-eastern TP, recorded the ice-free
432 season temperature, which was relatively stable during the Holocene ([Sun et al., 2021](#); [Zhang
433 et al., 2022a](#)). However, our temperature record from Gahai is different from the above
434 records and resembles summer temperature changes during the Holocene ([Chen et al., 2020](#)).
435 This is because the brGDGTs record from Lake Gahai represents warm season temperatures,
436 which adds to its reliability.



437

438 **Fig. 8** Comparison of Holocene temperature based on brGDGTs at Gahai (a) and other

439 records from around the TP. Reconstructed ice-free-season temperatures from (b)

440 Tingming lake (Sun et al., 2021), (c) Cuoqia lake (Zhang et al., 2022a). Reconstructed

441 annual temperature from (d) Lugu lake (Zhao et al., 2021b), (e) Tiancai lake (Feng et al.,

442 2022), (f) Ngamring Co (Sun et al., 2022), (g) Hongyuan peatland (Yan et al., 2021). (h)

443 Dangxiong wetland (Cheung et al., 2017), (i) Aweng Co (Li et al., 2017), (j) Bangong



444 Co (Wang et al., 2021c).

445

446 We suggest that the complexity of Holocene temperature patterns recorded by brGDGTs in
447 TP lakes is primarily due to the ambiguity of brGDGTs in these lakes, as well as to the spatial
448 heterogeneity of climate change across the TP. This ambiguity can be attributed to several
449 factors. First, the origin of brGDGTs in lakes remains an uncertain factor in temperature
450 reconstruction. An increasing number of studies indicate the occurrence of a significant
451 amount of autochthonous brGDGTs in lakes, but their abundance in soil can also affect the
452 distribution of brGDGTs in lakes due to their supply via soil erosion (e.g., Tierney and
453 Russell, 2009; Weber et al., 2015; Wang et al., 2023). In fact, even within the same lake (e.g.,
454 Tengchongqinghai lake in southwestern China), two studies reached inconsistent conclusions
455 regarding the origin of brGDGTs (Tian et al., 2019; Zhao et al., 2021b), possibly because the
456 niches of certain brGDGTs may expand or contract compared to other locations within a lake.
457 Therefore, it is important to conduct detailed modern process studies to accurately assess the
458 sources of brGDGTs in lakes, especially with regard to evaluating the proportion of
459 autochthonous brGDGTs (Martin et al., 2020; Wang et al., 2023). Second, brGDGTs may
460 show a seasonal signal. Current brGDGTs–temperature calibrations for lakes reflect the
461 annual average temperature (Sun et al., 2011; De Jonge et al., 2014), as well as the growing
462 season temperature (Sun et al., 2011; Dang et al., 2018) and the ice-free season temperature
463 (Martínez-Sosa et al., 2021; Zhang et al., 2022a). Thus, there is no consensus regarding
464 whether the brGDGTs have a seasonal bias, and it is necessary to conduct continuous, high-
465 resolution seasonal investigations of lakes on the Tibetan Plateau to comprehensively



466 elucidate the seasonal characteristics of brGDGTs. This can enhance the accuracy of regional
467 temperature reconstruction and may help reconcile the complex temperature patterns
468 observed on the Tibetan Plateau. Third, the factors affecting the distribution of brGDGTs in
469 lakes are complex, including not only temperature, pH and salinity but also oxygen content,
470 water depth, and so on (Wang et al., 2016; Wang et al., 2021b). The distribution of brGDGTs
471 in lakes is significantly influenced by the hydrological and physical properties of the lakes,
472 and thus it is necessary to attain a more comprehensive understanding of the characteristics of
473 the lakes in the study area and their effects on brGDGTs. Fourth, different brGDGTs–
474 temperature calibrations may lead to significant differences in both the amplitude and trend of
475 temperature from the same dataset (Wang et al., 2016; Feng et al., 2019). One reason for this
476 is the deviation between in-situ measured temperature and atmospheric temperature (Wang et
477 al., 2020). Thus, selecting an appropriate calibration and attempting to establish a brGDGTs-
478 in situ temperature calibration are effective means of enhancing the reliability of brGDGTs-
479 based temperature reconstructions.

480

481 **4 Conclusions**

482 We present a quantitative, brGDGTs-based seasonal paleotemperature record over the last 15
483 ka from the sediments of a shallow lake on the eastern Tibetan Plateau. Our reconstruction
484 resembles the summer temperature trend, with the Holocene Thermal Maximum occurring
485 during 8–3.5 ka. There is a lag between our brGDGTs-based reconstruction and pollen-based
486 July temperature recorded in the same sediment core, indicating a significant seasonal bias
487 between different proxies. Since 3.5 ka, the temperature decreased gradually, and the surficial



488 sediments reliably recorded the warm season temperature during the current period in the
489 Gahai Lake region. However, intensive local human activity during the last century has
490 affected the distribution of brGDGTs, resulting in temperature deviations recorded by
491 brGDGTs. However, the implementation of environmental protection policies have reduced
492 this anthropogenic signal. Our findings help better understand the seasonal signal of
493 brGDGTs in shallow lakes and provide important data for improving projections of terrestrial
494 climate change at high elevations.

495

496 We also investigated previously published brGDGTs-based Holocene temperature records on
497 the TP to determine the pattern of brGDGTs-based temperature changes and the possible
498 causes of the differences between reconstructions. We emphasize the need for the careful
499 examination of both the source and behavior of these compounds in lacustrine environments
500 and lake status, prior to the application of brGDGTs proxies in paleolimnological
501 reconstruction.

502

503 **Competing interests**

504 The contact author has declared that none of the authors has any competing interests.

505

506 **Acknowledgements**

507 This work was financially supported by the National Natural Science Foundation of China
508 (41877459) and the Second Tibetan Plateau Scientific Expedition and Research
509 (2019QZKK0601). We would like to thank Jan Bloemendal for the help with language



510 editing.

511



512 References

513

514 Bova, S., Rosenthal, Y., Liu, Z., Godad, S.P., Yan, M., 2021. Seasonal origin of the thermal maxima at the
515 Holocene and the last interglacial. *Nature* 589, 548-553.

516 Buckles, L.K., Weijers, J.W.H., Verschuren, D., Damste, J.S.S., 2014a. Sources of core and intact branched
517 tetraether membrane lipids in the lacustrine environment: Anatomy of Lake Challa and its catchment, equatorial
518 East Africa. *Geochimica Et Cosmochimica Acta* 140, 106-126.

519 Buckles, L.K., Weijers, J.W.H., Verschuren, D., Sinninghe Damsté, J.S., 2014b. Sources of core and intact
520 branched tetraether membrane lipids in the lacustrine environment: Anatomy of Lake Challa and its catchment,
521 equatorial East Africa. *Geochimica et Cosmochimica Acta* 140, 106-126.

522 Cao, J., Rao, Z., Shi, F., Jia, G., 2020. Ice formation on lake surfaces in winter causes warm-season bias of
523 lacustrine brGDGT temperature estimates. *Biogeosciences* 17, 2521-2536.

524 Cartapanis, O., Jonkers, L., Moffa-Sanchez, P., Jaccard, S.L., de Vernal, A., 2022. Complex spatio-temporal
525 structure of the Holocene Thermal Maximum. *Nat Commun* 13, 5662.

526 Chen, D., Xu, B., Yao, T., Guo, Z., Cui, P., Chen, F., Zhang, R., Zhang, X., Zhang, Y., Fan, J., Hou, Z., Zhang, T.,
527 2015. Assessment of past, present and future environmental changes on the Tibetan Plateau. *Chinese Science*
528 *Bulletin* 60, 3025-3035.

529 Chen, F., Yu, Z., Yang, M., Ito, E., Wang, S., Madsen, D.B., Huang, X., Zhao, Y., Sato, T., Birks, H.J.B., Boomer,
530 I., Chen, J., An, C., Wünnemann, B., 2008. Holocene moisture evolution in arid central Asia and its out-of-phase
531 relationship with Asian monsoon history. *Quaternary Science Reviews* 27, 351-364.

532 Chen, F., Zhang, J., Liu, J., Cao, X., Hou, J., Zhu, L., Xu, X., Liu, X., Wang, M., Wu, D., Huang, L., Zeng, T.,
533 Zhang, S., Huang, W., Zhang, X., Yang, K., 2020. Climate change, vegetation history, and landscape responses
534 on the Tibetan Plateau during the Holocene: A comprehensive review. *Quaternary Science Reviews* 243.

535 Chen, Y., Zheng, F., Yang, H., Yang, W., Wu, R., Liu, X., Liang, H., Chen, H., Pei, H., Zhang, C., Pancost, R.D.,
536 Zeng, Z., 2022. The production of diverse brGDGTs by an Acidobacterium providing a physiological basis for
537 paleoclimate proxies. *Geochimica et Cosmochimica Acta* 337, 155-165.

538 Cheung, M.-C., Zong, Y., Zheng, Z., Liu, Z., Aitchison, J.C., 2017. Holocene temperature and precipitation
539 variability on the central Tibetan Plateau revealed by multiple palaeo-climatic proxy records from an alpine
540 wetland sequence. *The Holocene* 27, 1669-1681.

541 Crampton-Flood, E.D., Tierney, J.E., Peterse, F., Kirkels, F.M.S.A., Damste, J.S.S., 2020. BayMBT: A Bayesian
542 calibration model for branched glycerol dialkyl glycerol tetraethers in soils and peats. *Geochimica Et*
543 *Cosmochimica Acta* 268, 142-159.

544 Damsté, J.S.S., Hopmans, E.C., Pancost, R.D., Schouten, S., Geenevasen, J.A.J., 2000. Newly discovered non-
545 isoprenoid glycerol dialkyl glycerol tetraether lipids in sediments. *Chemical Communications*, 1683-1684.

546 Damsté, J.S.S., Ossebaar, J., Abbas, B., Schouten, S., Verschuren, D., 2009. Fluxes and distribution of tetraether
547 lipids in an equatorial African lake: Constraints on the application of the TEX86 palaeothermometer and BIT
548 index in lacustrine settings. *Geochimica et Cosmochimica Acta* 73, 4232-4249.

549 Dang, X., Ding, W., Yang, H., Pancost, R.D., Naafs, B.D.A., Xue, J., Lin, X., Lu, J., Xie, S., 2018. Different
550 temperature dependence of the bacterial brGDGT isomers in 35 Chinese lake sediments compared to that in
551 soils. *Organic Geochemistry* 119, 72-79.

552 De Jonge, C., Hopmans, E.C., Zell, C.I., Kim, J.-H., Schouten, S., Sinninghe Damsté, J.S., 2014. Occurrence
553 and abundance of 6-methyl branched glycerol dialkyl glycerol tetraethers in soils: Implications for
554 palaeoclimate reconstruction. *Geochimica et Cosmochimica Acta* 141, 97-112.

555 Ding, S., Xu, Y., Wang, Y., He, Y., Hou, J., Chen, L., He, J.S., 2015. Distribution of branched glycerol dialkyl



- 556 glycerol tetraethers in surface soils of the Qinghai-Tibetan Plateau: implications of brGDGTs-based proxies in
557 cold and dry regions. *Biogeosciences* 12, 3141-3151.
- 558 Dong, Y., Wu, N., Li, F., Zhang, D., Zhang, Y., Shen, C., Lu, H., 2022. The Holocene temperature conundrum
559 answered by mollusk records from East Asia. *Nat Commun* 13, 5153.
- 560 Dyke, A.S., 2004. An outline of North American deglaciation with emphasis on central and northern Canada.
561 *Quaternary Glaciations-Extent and Chronology, Pt 2: North America* 2, 373-424.
- 562 Dykoski, C.A., Edwards, R.L., Cheng, H., Yuan, D.X., Cai, Y.J., Zhang, M.L., Lin, Y.S., Qing, J.M., An, Z.S.,
563 Revenaugh, J., 2005. A high-resolution, absolute-dated Holocene and deglacial Asian monsoon record from
564 Dongge Cave, China. *Earth and Planetary Science Letters* 233, 71-86.
- 565 Feng, X., Zhao, C., D'Andrea, W.J., Hou, J., Yang, X., Xiao, X., Shen, J., Duan, Y., Chen, F., 2022. Evidence for
566 a Relatively Warm Mid-to Late Holocene on the Southeastern Tibetan Plateau. *Geophysical Research Letters* 49.
- 567 Feng, X., Zhao, C., D'Andrea, W.J., Liang, J., Zhou, A., Shen, J., 2019. Temperature fluctuations during the
568 Common Era in subtropical southwestern China inferred from brGDGTs in a remote alpine lake. *Earth and*
569 *Planetary Science Letters* 510, 26-36.
- 570 Günther, F., Thiele, A., Gleixner, G., Xu, B., Yao, T., Schouten, S., 2014. Distribution of bacterial and archaeal
571 ether lipids in soils and surface sediments of Tibetan lakes: Implications for GDGT-based proxies in saline high
572 mountain lakes. *Organic Geochemistry* 67, 19-30.
- 573 Halamka, T.A., Raberg, J.H., McFarlin, J.M., Younkin, A.D., Mulligan, C., Liu, X.L., Kopf, S.H., 2022.
574 Production of diverse brGDGTs by *Acidobacterium Solibacter usitatus* in response to temperature, pH, and O₂
575 provides a culturing perspective on brGDGT proxies and biosynthesis. *Geobiology*.
- 576 He, Y., Hou, J., Wang, M., Li, X., Liang, J., Xie, S., Jin, Y., 2020. Temperature Variation on the Central Tibetan
577 Plateau Revealed by Glycerol Dialkyl Glycerol Tetraethers From the Sediment Record of Lake Linggo Co Since
578 the Last Deglaciation. *Frontiers in Earth Science* 8.
- 579 Herzschuh, U., Borkowski, J., Schewe, J., Mischke, S., Tian, F., 2014. Moisture-advection feedback supports
580 strong early-to-mid Holocene monsoon climate on the eastern Tibetan Plateau as inferred from a pollen-based
581 reconstruction. *Palaeogeography, Palaeoclimatology, Palaeoecology* 402, 44-54.
- 582 Hou, J., Huang, Y., Zhao, J., Liu, Z., Colman, S., An, Z., 2016. Large Holocene summer temperature oscillations
583 and impact on the peopling of the northeastern Tibetan Plateau. *Geophysical Research Letters* 43, 1323-1330.
- 584 Hou, J., Li, C., Lee, S., 2019. The temperature record of the Holocene: progress and controversies. *Science*
585 *Bulletin*.
- 586 Huguot, C., Hopmans, E.C., Febo-Ayala, W., Thompson, D.H., Sinninghe Damsté, J.S., Schouten, S., 2006. An
587 improved method to determine the absolute abundance of glycerol dibiphytanyl glycerol tetraether lipids.
588 *Organic Geochemistry* 37, 1036-1041.
- 589 Kuang, X., Jiao, J.J., 2016. Review on climate change on the Tibetan Plateau during the last half century.
590 *Journal of Geophysical Research: Atmospheres* 121, 3979-4007.
- 591 Laskar, J., Robutel, P., Joutel, F., Gastineau, M., Correia, A.C.M., Levrard, B., 2004. A long-term numerical
592 solution for the insolation quantities of the Earth. *Astronomy & Astrophysics* 428, 261-285.
- 593 Li, X., Wang, M., Zhang, Y., Lei, L., Hou, J., 2017. Holocene climatic and environmental change on the western
594 Tibetan Plateau revealed by glycerol dialkyl glycerol tetraethers and leaf wax deuterium-to-hydrogen ratios at
595 Aweng Co. *Quaternary Research* 87, 455-467.
- 596 Liu, Y., Zhang, M., Liu, Z., Xia, Y., Huang, Y., Peng, Y., Zhu, J., 2018. A Possible Role of Dust in Resolving the
597 Holocene Temperature Conundrum. *Scientific Reports* 8.
- 598 Liu, Z.Y., Zhu, J., Rosenthal, Y., Zhang, X., Otto-Bliesner, B.L., Timmermann, A., Smith, R.S., Lohmann, G.,
599 Zheng, W.P., Timm, O.E., 2014. The Holocene temperature conundrum. *Proc. Natl. Acad. Sci. U. S. A.* 111,



- 600 E3501-E3505.
- 601 Loomis, S.E., Russell, J.M., Ladd, B., Street-Perrott, F.A., Sinninghe Damsté, J.S., 2012. Calibration and
602 application of the branched GDGT temperature proxy on East African lake sediments. *Earth and Planetary
603 Science Letters* 357-358, 277-288.
- 604 Lu, H., Liu, W., Yang, H., Wang, H., Liu, Z., Leng, Q., Sun, Y., Zhou, W., An, Z., 2019. 800-kyr land
605 temperature variations modulated by vegetation changes on Chinese Loess Plateau. *Nat Commun* 10, 1958.
- 606 Lu, H., Wu, N., Liu, K.-b., Zhu, L., Yang, X., Yao, T., Wang, L., Li, Q., Liu, X., Shen, C., Li, X., Tong, G., Jiang,
607 H., 2011. Modern pollen distributions in Qinghai-Tibetan Plateau and the development of transfer functions for
608 reconstructing Holocene environmental changes. *Quaternary Science Reviews* 30, 947-966.
- 609 Ma, W., Li, G., Song, J., Yan, L., Wu, L., 2019. Effect of Vegetation Degradation on Soil Organic Carbon Pool
610 and Carbon Pool Management Index in the Gahai Wetland, China. *Acta Agrestia Sinica* 27, 687-694.
- 611 Marcott, S.A., Shakun, J.D., Clark, P.U., Mix, A.C., 2013. A Reconstruction of Regional and Global
612 Temperature for the Past 11,300 Years. *Science* 339, 1198-1201.
- 613 Marsicek, J., Shuman, B.N., Bartlein, P.J., Shafer, S.L., Brewer, S., 2018. Reconciling divergent trends and
614 millennial variations in Holocene temperatures. *Nature* 554, 92-+.
- 615 Martin, C., Ménot, G., Thouveny, N., Peyron, O., Andrieu-Ponel, V., Montade, V., Davtian, N., Reille, M., Bard,
616 E., 2020. Early Holocene Thermal Maximum recorded by branched tetraethers and pollen in Western Europe
617 (Massif Central, France). *Quaternary Science Reviews* 228, 106109.
- 618 Martínez-Sosa, P., Tierney, J.E., Stefanescu, I.C., Dearing Crampton-Flood, E., Shuman, B.N., Routson, C.,
619 2021. A global Bayesian temperature calibration for lacustrine brGDGTs. *Geochimica et Cosmochimica Acta*
620 305, 87-105.
- 621 Moser, K.A., Baron, J.S., Brahney, J., Oleksy, I.A., Saros, J.E., Hundey, E.J., Sadro, S., Kopáček, J., Sommaruga,
622 R., Kainz, M.J., Strecker, A.L., Chandra, S., Walters, D.M., Preston, D.L., Michelutti, N., Lepori, F., Spaulding,
623 S.A., Christianson, K.R., Melack, J.M., Smol, J.P., 2019. Mountain lakes: Eyes on global environmental change.
624 *Global and Planetary Change* 178, 77-95.
- 625 Opitz, S., Zhang, C., Herzschuh, U., Mischke, S., 2015. Climate variability on the south-eastern Tibetan Plateau
626 since the Lateglacial based on a multiproxy approach from Lake Naleng – comparing pollen and non-pollen
627 signals. *Quaternary Science Reviews* 115, 112-122.
- 628 Pang, H., Hou, S., Zhang, W., Wu, S., Jenk, T.M., Schwikowski, M., Jouzel, J., 2020. Temperature Trends in the
629 Northwestern Tibetan Plateau Constrained by Ice Core Water Isotopes Over the Past 7,000 Years. *Journal of
630 Geophysical Research-Atmospheres* 125.
- 631 Peterse, F., Vonk, J.E., Holmes, R.M., Giosan, L., Zimov, N., Eglinton, T.I., 2014. Branched glycerol dialkyl
632 glycerol tetraethers in Arctic lake sediments: Sources and implications for paleothermometry at high latitudes.
633 *Journal of Geophysical Research: Biogeosciences* 119, 1738-1754.
- 634 Qiu, J., 2008. The third pole. *Nature* 454, 393-396.
- 635 Russell, J.M., Hopmans, E.C., Loomis, S.E., Liang, J., Sinninghe Damsté, J.S., 2018. Distributions of 5- and 6-
636 methyl branched glycerol dialkyl glycerol tetraethers (brGDGTs) in East African lake sediment: Effects of
637 temperature, pH, and new lacustrine paleotemperature calibrations. *Organic Geochemistry* 117, 56-69.
- 638 Shanahan, T.M., Hughen, K.A., Van Mooy, B.A.S., 2013. Temperature sensitivity of branched and isoprenoid
639 GDGTs in Arctic lakes. *Organic Geochemistry* 64, 119-128.
- 640 Sun, Q., Chu, G., Liu, M., Xie, M., Li, S., Ling, Y., Wang, X., Shi, L., Jia, G., Lü, H., 2011. Distributions and
641 temperature dependence of branched glycerol dialkyl glycerol tetraethers in recent lacustrine sediments from
642 China and Nepal. *Journal of Geophysical Research* 116.
- 643 Sun, X., Zhao, C., Zhang, C., Feng, X., Yan, T., Yang, X., Shen, J., 2021. Seasonality in Holocene Temperature



- 644 Reconstructions in Southwestern China. *Paleoceanography and Paleoclimatology* 36.
- 645 Sun, Z., Hou, X., Ji, K., Yuan, K., Li, C., Wang, M., Hou, J., 2022. Potential winter-season bias of annual
646 temperature variations in monsoonal Tibetan Plateau since the last deglaciation. *Quaternary Science Reviews*
647 292.
- 648 Thompson, L.G., Yao, T., Davis, M.E., Henderson, K.A., MosleyThompson, E., Lin, P.N., Beer, J., Synal, H.A.,
649 ColeDai, J., Bolzan, J.F., 1997. Tropical climate instability: The last glacial cycle from a Qinghai-Tibetan ice
650 core. *Science* 276, 1821-1825.
- 651 Tian, L., Wang, M., Zhang, X., Yang, X., Zong, Y., Jia, G., Zheng, Z., Man, M., 2019. Synchronous change of
652 temperature and moisture over the past 50 ka in subtropical southwest China as indicated by biomarker records
653 in a crater lake. *Quaternary Science Reviews* 212, 121-134.
- 654 Tierney, J.E., Russell, J.M., 2009. Distributions of branched GDGTs in a tropical lake system: Implications for
655 lacustrine application of the MBT/CBT paleoproxy. *Organic Geochemistry* 40, 1032-1036.
- 656 Tierney, J.E., Russell, J.M., Eggermont, H., Hopmans, E.C., Verschuren, D., Sinninghe Damsté, J.S., 2010.
657 Environmental controls on branched tetraether lipid distributions in tropical East African lake sediments.
658 *Geochimica et Cosmochimica Acta* 74, 4902-4918.
- 659 Wang, G., Wang, Y., Wei, Z., He, W., Ma, X., Zhang, T., 2021a. Reconstruction of temperature and precipitation
660 spanning the past 28 kyr based on branched tetraether lipids from Qionghai Lake, southwestern China.
661 *Palaeogeography Palaeoclimatology Palaeoecology* 562.
- 662 Wang, H., An, Z., Lu, H., Zhao, Z., Liu, W., 2020. Calibrating bacterial tetraether distributions towards in situ
663 soil temperature and application to a loess-paleosol sequence. *Quaternary Science Reviews* 231.
- 664 Wang, H., Chen, W., Zhao, H., Cao, Y., Hu, J., Zhao, Z., Cai, Z., Wu, S., Liu, Z., Liu, W., 2023. Biomarker-
665 based quantitative constraints on maximal soil-derived brGDGTs in modern lake sediments. *Earth and Planetary*
666 *Science Letters* 602.
- 667 Wang, H., Liu, W., He, Y., Zhou, A., Zhao, H., Liu, H., Cao, Y., Hu, J., Meng, B., Jiang, J., Kolpakova, M.,
668 Krivonogov, S., Liu, Z., 2021b. Salinity-controlled isomerization of lacustrine brGDGTs impacts the associated
669 MBT5ME' terrestrial temperature index. *Geochimica et Cosmochimica Acta* 305, 33-48.
- 670 Wang, M., Liang, J., Hou, J., Hu, L., 2016. Distribution of GDGTs in lake surface sediments on the Tibetan
671 Plateau and its influencing factors. *Science China Earth Sciences* 59, 961-974.
- 672 Wang, M.D., Hou, J.Z., Duan, Y.W., Chen, J.H., Li, X.M., He, Y., Lee, S.Y., Chen, F.H., 2021c. Internal
673 feedbacks forced Middle Holocene cooling on the Qinghai-Tibetan Plateau. *Boreas*.
- 674 Wang, N., Liu, L., Hou, X., Zhang, Y., Wei, H., Cao, X., 2022. Palynological evidence reveals an arid early
675 Holocene for the northeast Tibetan Plateau. *Climate of the Past* 18, 2381-2399.
- 676 Weber, Y., De Jonge, C., Rijkstra, W.I.C., Hopmans, E.C., Stadnitskaia, A., Schubert, C.J., Lehmann, M.F.,
677 Sinninghe Damsté, J.S., Niemann, H., 2015. Identification and carbon isotope composition of a novel branched
678 GDGT isomer in lake sediments: Evidence for lacustrine branched GDGT production. *Geochimica et*
679 *Cosmochimica Acta* 154, 118-129.
- 680 Weijers, J.W.H., Schouten, S., van den Donker, J.C., Hopmans, E.C., Sinninghe Damsté, J.S., 2007.
681 Environmental controls on bacterial tetraether membrane lipid distribution in soils. *Geochimica et*
682 *Cosmochimica Acta* 71, 703-713.
- 683 Woltering, M., Werne, J.P., Kish, J.L., Hicks, R., Sinninghe Damsté, J.S., Schouten, S., 2012. Vertical and
684 temporal variability in concentration and distribution of thaumarchaeotal tetraether lipids in Lake Superior and
685 the implications for the application of the TEX86 temperature proxy. *Geochimica et Cosmochimica Acta* 87,
686 136-153.
- 687 Wu, D., Chen, X., Lv, F., Brenner, M., Curtis, J., Zhou, A., Chen, J., Abbott, M., Yu, J., Chen, F., 2018.



- 688 Decoupled early Holocene summer temperature and monsoon precipitation in southwest China. *Quaternary*
689 *Science Reviews* 193, 54-67.
- 690 Yan, T., Zhao, C., Yan, H., Shi, G., Sun, X., Zhang, C., Feng, X., Leng, C., 2021. Elevational differences in
691 Holocene thermal maximum revealed by quantitative temperature reconstructions at ~30° N on eastern Tibetan
692 Plateau. *Palaeogeography, Palaeoclimatology, Palaeoecology* 570, 110364.
- 693 Yao, T., Bolch, T., Chen, D., Gao, J., Immerzeel, W., Piao, S., Su, F., Thompson, L., Wada, Y., Wang, L., Wang,
694 T., Wu, G., Xu, B., Yang, W., Zhang, G., Zhao, P., 2022. The imbalance of the Asian water tower. *Nature*
695 *Reviews Earth & Environment* 3, 618-632.
- 696 Zhang, C., Zhao, C., Yu, S.-Y., Yang, X., Cheng, J., Zhang, X., Xue, B., Shen, J., Chen, F., 2022a. Seasonal
697 imprint of Holocene temperature reconstruction on the Tibetan Plateau. *Earth-Science Reviews* 226, 103927.
- 698 Zhang, E., Chang, J., Cao, Y., Sun, W., Shulmeister, J., Tang, H., Langdon, P.G., Yang, X., Shen, J., 2017.
699 Holocene high-resolution quantitative summer temperature reconstruction based on subfossil chironomids from
700 the southeast margin of the Qinghai-Tibetan Plateau. *Quaternary Science Reviews* 165, 1-12.
- 701 Zhang, E., Chang, J., Shulmeister, J., Langdon, P., Sun, W., Cao, Y., Yang, X., Shen, J., 2019a. Summer
702 temperature fluctuations in Southwestern China during the end of the LGM and the last deglaciation. *Earth and*
703 *Planetary Science Letters* 509, 78-87.
- 704 Zhang, G., Luo, W., Chen, W., Zheng, G., 2019b. A robust but variable lake expansion on the Tibetan Plateau.
705 *Science Bulletin* 64, 1306-1309.
- 706 Zhang, W., Wu, H., Cheng, J., Geng, J., Li, Q., Sun, Y., Yu, Y., Lu, H., Guo, Z., 2022b. Holocene seasonal
707 temperature evolution and spatial variability over the Northern Hemisphere landmass. *Nat Commun* 13, 5334.
- 708 Zhao, B., Castaneda, I.S., Bradley, R.S., Salacup, J.M., de Wet, G.A., Daniels, W.C., Schneider, T., 2021a.
709 Development of an in situ branched GDGT calibration in Lake 578, southern Greenland. *Organic Geochemistry*
710 152.
- 711 Zhao, C., Liu, Z.H., Rohling, E.J., Yu, Z.C., Liu, W.G., He, Y.X., Zhao, Y., Chen, F.H., 2013. Holocene
712 temperature fluctuations in the northern Tibetan Plateau. *Quaternary Research* 80, 55-65.
- 713 Zhao, C., Rohling, E.J., Liu, Z., Yang, X., Zhang, E., Cheng, J., Liu, Z., An, Z., Yang, X., Feng, X., Sun, X.,
714 Zhang, C., Yan, T., Long, H., Yan, H., Yu, Z., Liu, W., Yu, S.-Y., Shen, J., 2021b. Possible obliquity-forced
715 warmth in southern Asia during the last glacial stage. *Science Bulletin* 66, 1136-1145.
- 716 Zheng, Y., Li, Q., Wang, Z., Naafs, B.D.A., Yu, X., Pancost, R.D., 2015. Peatland GDGT records of Holocene
717 climatic and biogeochemical responses to the Asian Monsoon. *Organic Geochemistry* 87, 86-95.
- 718 Zhou, W., Yu, S.-Y., Burr, G.S., Kukla, G.J., Jull, A.J.T., Xian, F., Xiao, J., Colman, S.M., Yu, H., Liu, Z., Kong,
719 X., 2010. Postglacial changes in the Asian summer monsoon system: a pollen record from the eastern margin of
720 the Tibetan Plateau. *Boreas* 39, 528-539.
- 721 Zielinski, G.A., Mershon, G.R., 1997. Paleoenvironmental implications of the insoluble microparticle record in
722 the GISP2 (Greenland) ice core during the rapidly changing climate of the Pleistocene-Holocene transition.
723 *Geological Society of America Bulletin* 109, 547-559.
- 724
- 725